Prussian blue immobilized on covalent organic polymer-grafted granular activated carbon for cesium adsorption from water

Younggyo Seo, Yuhoon Hwang [*]

Department of Environmental Engineering, Seoul National University of Science and Technology, Seoul 01811, Republic of Korea

A B S T R A C T

Technologies for removing radioactive waste in the form of ^{137}Cs, released during nuclear power plant accidents, are essential. Prussian blue (PB) is a pigment with a face-centered cubic structure that can selectively adsorb cesium. However, due to its very small size (5–200 nm), PB can be found in water as a fine powder and it is difficult to separate its disposal to the water system. Thus, in this study, PB was immobilized on granular activated carbon (GAC), normally used for water treatment, to facilitate its recovery after usage. The GAC surface was grafted with a covalent organic polymer (COP) to improve its stability and prevent PB desorption. The COP-grafted GAC immobilized approximately twice as much PB as the ungrafted one; its cesium adsorption capacity was over three times higher and the PB stability was excellent. The effects of pH and water matrix were investigated using samples of both artificial and actual river water. Moreover, a continuous column experiment was conducted to evaluate the applicability of the proposed material in water treatment system in a form of GAC column.

1. Introduction

Over the past few centuries, civilizations have advanced rapidly through industrialization and economic growth; however, the energy demand and consumption have risen accordingly [1,2]. Thus, the issues of fossil fuel depletion and environmental pollution have gradually emerged. Therefore, many countries have adopted nuclear energy as an alternative and eco-friendly solution. Hence, the number of nuclear power plants has continuously risen, especially from 1998 to 2018; As of 2018, 454 plants are currently operating in 30 countries and other 54 are under construction [3]. Nuclear energy is an optimal energy source in terms of economic efficiency and stability, but the operation, repairing, and disposal of nuclear power plants generate harmful radioactive pollutants [4,5]. The radioactive waste released during the nuclear accidents of Chernobyl (1986) and Fukushima (2011) has seriously affected the environment; such events have raised serious concerns about the use of nuclear energy.

The radioactive waste generated during nuclear power plant accidents generally consists of several radioisotopes, which are unstable elements detrimental to humans and the environment because they emit ionizing radiation while decaying [6]. The main radioisotopes released in such events are strontium, cesium, and iodine. Among them, cesium

has 30 isotopes with atomic weights between 112 and 151; some of them occur naturally, while others are produced through nuclear reactions. Its main radioisotope is ^{137}Cs, which has a half-life of 30.2 years [7,8]. ^{137}Cs is dangerous because it can cause secondary pollution by entering surface water through fallout. Therefore, various methods to remove radioactive cesium have been developed so far, including adsorption, solvent extraction, ion exchange, coprecipitation, reverse osmosis, and membrane filtration [9–12]. Adsorption is the most used technique due to the simple procedure, cost-effectiveness, negligible secondary pollution; zeolites, graphene oxide, ammonium molybdophosphate Prussian blue (PB) are the most common adsorbents of radioactive cesium [13–17]. The spent adsorbent is considered radioactive waste. Therefore, the spent adsorbent volume is an issue during its disposal. The overall volume is significantly reduced through adsorption since it is much more concentrated than the contaminated water, which contains few pg/L to μg/L of radioactive matter.

PB is a classic example of a mixed-valence iron(II)–iron(III) inorganic complex with a face-centered cubic structure that can selectively adsorb alkali cations [18–20]. Its lattice constant is 10.17 Å, and the average distances are Fe(II)-C = 1.92 Å, C-N = 1.13 Å, and Fe(III)-N = 2.03 Å [21]. Since its cubic lattice size is similar to that of cesium ions, PB can selectively adsorb Cs compared to other alkali cations [22]. The

Cs-adsorption mechanisms can be divided into physical and chemical adsorption. Physical adsorption is related to the ionic radius of the target alkali metal and the hydration degree. Because the hydrated radius of Cs (1.19 Å) is smaller than that of other alkali metals (K$^+$: 1.25 Å; Na$^+$: 1.84 Å) and because it is the best suited to fit the PB lattice structure during hydration, its physical adsorption strength is higher than that of other alkali cations (Cs$^+$ ≫ K$^+$ ≥ Na$^+$) [23]. In chemical adsorption, the water molecules are coordinated and hydrophilic inside the PB lattice structure; thus, hydrated Cs$^+$ is easily adsorbed into these hydrophilic spaces, getting immobilized via the proton exchange between water molecules and Fe ions [24]. Therefore, PB can selectively remove cesium both physically and chemically.

However, PB is generally present as an ultrafine powder in water due to its dispersibility, hydrophilicity, and very small particle size (5–200 nm); this hinders its separation from water after its usage as Cs adsorbent and limits its use in the treatment of actual water [25,26]. Therefore, a method for the PB immobilization on some support materials, to prevent its dispersion in water and facilitate its recovery, is required. In this regard, several studies have investigated granular filtering materials as PB immobilizers that allow water treatments. Granular activated carbon (GAC) is the most commonly used among them for this purpose due to its high specific surface area [27,28]. However, the earlier reports did not focus on the PB desorption, which could cause secondary pollution in water treatment systems.

In previous studies, we used fibrous filters as supporting materials for PB, demonstrating the effectiveness of surface functionalization; the polymerization of acrylic acid on a cellulose filter or a polyvinyl alcohol sponge enhanced the PB immobilization [29,30]. In the present study, we grafted a porous organic polymer on GAC to provide physical and chemical advantages for the PB immobilization. The used polymer was a covalent organic polymer (COP) formed through a substitution reaction of cyanuric chloride and aromatic nuclear substitution. Due to its net-like structure, it provided the GAC surface with a large surface area and mesopores. The activated carbon contained only micropores, and the larger pores (2.6–10 nm) were generated by the COP structure itself. The used COP is stable in extreme environments (e.g., high temperatures and pressures) and is already used as an adsorbent for dyes, cadmium ions, and iron ions [31]. We expected a stable immobilization of PB on this COP-grafted GAC (GAC-COP) because its nanoporous nature should capture both the PB and the amine functional groups interacting with the iron ions, the PB precursors. The similar approach was used to immobilize PB on COP-grafted powdered activated carbon (PAC-COP) in our previous study [32]. The binding matrix, that is, COP, increased the immobilization stability of PB on the activated carbon surface. Moreover, the immobilization of a larger quantity of PB enhanced the cesium adsorption performance. However, the use of PAC-COP-PB in practical applications was not well investigated.

Then, the Prussian blue that can selectively remove radioactive cesium and COPs were synthesized on GAC's surface. Furthermore, the immobilization and elution characteristics of the PB fixed on the GAC-COP were evaluated. Then, the resulting composite, that is, PB immobilized on GAC-COP (GAC-COP-PB), was tested as a Cs adsorbent, and its performance was assessed by conducting adsorption isotherm tests. The stable isotope ^{133}Cs was used instead of ^{137}Cs because of safety issues. The effects of pH and water matrix were investigated using artificial and actual stream water samples. A continuous column experiment was also conducted to assess the applicability of the proposed material.

2. Materials and methods

2.1. Chemicals and equipment

2.1.1. Chemicals

Activated carbon (granular), iron (III) chloride, hydrochloric acid (35%), sodium hydroxide (99%), magnesium chloride hexahydrate (98%), calcium chloride dihydrate (71–77.5%), calcium nitrate

tetrahydrate (98%), calcium carbonate (99%), sodium sulfate (99%), potassium bicarbonate (99%), sodium bicarbonate (99%), and magnesium sulfate heptahydrate (99%) were obtained from Duksan Chemical Co. (Ansan-si, Gyeonggi-do, Republic of Korea). Nitric acid (60%), sulfuric acid (98%), dichloromethane (99%), thionyl chloride (99%), melamine (99%), dimethyl sulfoxide (99%), *N.N*-diisopropylethylamine (99%), and potassium ferrocyanide (99%) were obtained from Samchun Chemical Co. (Pyeongtaek, Gyeonggi-do, Republic of Korea). Terephthaldehyde (99%) was obtained from Sigma-Aldrich (St. Louis, MO, USA). Cesium standard solution (1000 ppm) was obtained from Kanto Chemical Co. (Chuo-ku, Tokyo, Japan).

2.1.2. Equipment

The adsorbent morphology was observed using a scanning electron microscope (SEM, SU8010, Hitachi High Technologies Corporation, Japan) coupled with an energy-dispersive spectrometer. The functional groups of the adsorbent were characterized using Fourier transform infrared spectroscope (FTIR, Nicolet iS50, Thermo Fisher Scientific, USA). The ion concentrations in soft, hard, and real stream waters were measured using an atomic absorption spectrometer (AAS, Elemental SOLAAR M6, Thermo Fisher Scientific, USA) and an ion chromatograph (IC, Aquion, Thermo Fisher Scientific, USA). The cesium concentration was measured with the inductively coupled plasma-mass spectroscopy technique (ICP-MS, NexION 350D, Perkin-Elmer, USA). The PB concentration in the aqueous system was confirmed using a UV–visible spectrophotometer (UV-Vis, Libara S22, BioChrom Ltd., USA).

2.2. GAC-COP-PB preparation and characterization

2.2.1. COP grafting on GAC

The grafting process was conducted as described in our previous works [31,33], through four main steps. The overall COP grafting process is presented in Fig. 1(a).

In step 1, the GAC (30 g) was oxidized by being mixed with an acid solution consisting of 30%HNO$_3$/47%H$_2$SO$_4$ at a ratio of 3:1. Then, this mixture was stirred at 350 rpm for 24 h to form hydroxyl and carboxyl groups on the GAC surface; the oxidized GAC (GAC-Ox) was washed with deionized water until reaching neutral pH and dried at 110 □.

In step 2, dichloromethane (400 mL) and thionyl chloride (100 mL) were added to 20 g of GAC-Ox to yield acyl chloride, followed by stirring at 350 rpm and 35 □ under nitrogen atmosphere for 24 h. In this process, the hydroxyl and carboxyl groups of the GAC-Ox are replaced with –OCl ends.

In step 3, immediately after step 2, the resulting solution was evaporated using a rotary evaporator before proceeding with melamine attachment. Then, melamine (2 g) dissolved in 500 mL of dimethyl sulfoxide (DMSO) and diisopropylethylamine (10 mL) were added to the solution, followed by stirring at 400 rpm and 120 □ for 24 h under nitrogen atmosphere. Next, the GAC was washed with DMSO and dried at 110 □.

In step 4, for COP reforming, melamine (1.25 g), terephthalaldehyde (2 g), and DMSO (500 mL) were added to 20 g of the melamine-attached GAC and reacted at 450 rpm and 150 □ for 24 h under nitrogen atmosphere. Then, the as-obtained GAC-COP was washed with DMSO and dried at 110 □.

2.2.2. PB immobilization

PB was immobilized through the following reaction in the presence of GAC-COP [23]. The overall scheme for in-situ PB synthesis is presented in Fig. 1(b).

$$4FeCl_3 + 3K_4[Fe(CN)_6] \rightarrow Fe_4[Fe(CN)_6]_3 + 12KCl \tag{1}$$
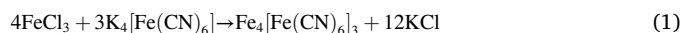
In practice, the GAC-COP (5 g) and 20 mM FeCl$_3$ (50 mL) were put into a 50 mL conical tube and stirred for 1 h with a vertical stirrer to induce Fe^{3+} adsorption. Then, the mixture was transferred into an Erlenmeyer flask and stirred at 300 rpm with a magnetic stirrer while
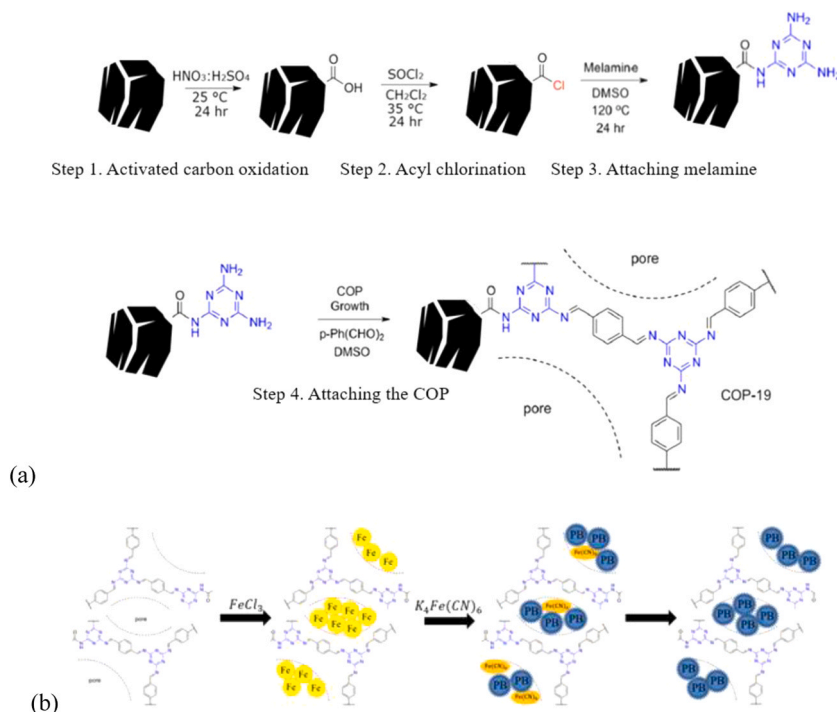
Fig. 1. (a) Schematic of COP grafting on GAC surface and (b) schematic of in-situ PB synthesis in GAC-COP.

injecting 20 mM $K_4Fe(CN)_6$ at a rate of 1 mL/min for 10 min, followed by further stirring for 50 min. Afterward, the mixture was washed with deionized water and dried in a vacuum oven, obtaining GAC-COP-PB. For comparison, PB was prepared using a similar method on the ungrafted GAC-Ox (GAC-PB) to verify the effect of COP grafting on PB immobilization.

2.2.3. Material characterization

A SEM-EDS was used to observe the surface morphology and elemental composition of the prepared materials; to ensure accuracy and reliability in the EDS results, the elemental analysis was conducted on the entire area of a single GAC grain. Moreover, the adsorbent surface's functional groups were determined using a FTIR spectrometer.

2.3. Adsorption performance evaluation

Since radioactive cesium is subject to many limitations and risks, our experiments were conducted using the stable isotope [133]Cs, which has similar properties as [137]Cs [34]. All of the adsorption tests were performed by adding specific amounts of an adsorbent into the [133]Cs solution, followed by stirring at a constant temperature in an incubator shaker. After the adsorption, the supernatant was collected, filtrated through a polyethersulfone membrane, and stored. The samples were diluted with 1% nitric acid and further analyzed using an ICP-MS.

2.3.1. Effect of COP on PB attachment

As a screening test, we evaluated the cesium adsorption efficiency of GAC, GAC-PB, GAC-COP, and GAC-COP-PB with an adsorbent dosage of 20 g/L and an initial [133]Cs concentration of 5 mg/L. After stirring for 24 h, the cesium removal rate was assessed via ICP-MS. To evaluate the adsorbent stability, we monitored the PB detachment from the GAC-PB and GAC-COP-PB samples. Different dosages of these adsorbents (1, 10, and 100 g/L) were added into deionized water; after stirring for 24 h, the amount of PB eluted was measured through absorbance analysis at 690 nm by using an UV-Vis and quantified with a calibration curve.

2.3.2. Adsorption kinetics

Kinetic experiments were conducted using the GAC-PB and GAC-COP-PB to understand how the COP grafting altered the adsorption rate and capacity. Each adsorbent (1 g) was injected into a 50-mL conical tube containing a 5 mg/L [133]Cs solution. The pH was not adjusted, and the mixture was continuously shaken at 30 ☐ for 24 h. The supernatant (2 mL) was aliquoted in a predetermined time interval, and the remaining [133]Cs concentration was measured with ICP-MS. The adsorption data were fitted using the pseudo-first-order and pseudo-second-order kinetics suggested by Lagergren, and Ho and McKay, respectively [35].

The linear forms of the two kinetics can be expressed as follows:

$$\ln(q_e - q_t) = \ln q_e - k_1 t \tag{2}$$

where q_e and q_t are the amounts of cesium ions adsorbed per unit weight of solid adsorbent (in mg/g) at time t, and k_1 is the adsorption rate constant (in L/min).

$$\frac{t}{q_t} = \frac{1}{k_2 q_e^2} + \left(\frac{1}{q_e}\right) \tag{3}$$

where k_2 is the rate constant (in g/mg·min).

2.3.3. Adsorption isotherms

An adsorption isotherm test was conducted to predict the adsorption capacity of the prepared materials. Identical amounts of GAC-PB and GAC-COP-PB (0.3 g) were added into a 15-mL conical tube in which the initial [133]Cs concentration was 1–70 mg/L. The pH was not adjusted, and the mixture was continuously shaken at 30 ☐ for 24 h. The supernatant (2 mL) was aliquoted at 24 h, and the concentration of the remaining [133]Cs was measured using an ICP-MS.

The adsorption isotherm of the adsorbed cesium ion at the equilibrium (q_e) was calculated using the Langmuir and Freundlich equations (Eqs. (4) and (5), respectively) as follows [36,37]:

$$q_e = \frac{q_m K_L C_e}{1 + K_L C_e} \tag{4}$$

where q_m is the maximum adsorption capacity of the adsorbent (in mg/g), C_e is the equilibrium concentration of the adsorbate in the solution (in mg/L), and K_L is the Langmuir affinity constant.

$$q_e = kC_e^{1/n} \qquad (5)$$

where k and $1/n$ are constants indicating the adsorption capacity and intensity, respectively.

2.3.4. Effects of initial pH and water matrix on ^{133}Cs adsorption

The effect of the initial pH was investigated using a 5 mg/L cesium solution at different initial pH values (4, 6, 8, and 10); the pH was controlled by adding 1 M HCl and 1 M NaOH solutions. The effect of the water matrix was evaluated by utilizing four types of water: deionized water, synthetic soft and hard water (to represent surface water and groundwater, respectively) [38], and real stream water from the Hallyu River in Goyang-si (Gyeonggi-do, Republic of Korea); the compositions of these samples are summarized in Table 1. The hardness values of soft water, hard water, and real stream water were 32.5, 163.3, and 114.3 mg $CaCO_3$/L, respectively. Both synthetic water samples contained various cations, including Ca^{2+}, Na^+, and K^+, that can compete with Cs^+. In all the tests, the adsorbent dosage was 20 g/L.

2.3.5. Continuous column experiment

This test was conducted to simulate the scenario where a cesium solution passes through a GAC column. First, the column was prepared by filling a glass column (2.5-cm diameter and 30-cm length) with 3 g of GAC-PB or GAC-COP-PB; the effective length was 4.5 cm. Then, a 200 µg/L ^{133}Cs solution was introduced into the column in an upward direction. The flow rate was maintained at 0.2 mL/min and 2 mL/min; therefore, the corresponding contact times were approximately 25 min and 2.5 min. A fraction collector periodically collected samples, and the cesium concentration in the effluent was evaluated through ICP–MS. The data obtained in a continuous column operation were used to calculate the maximum adsorption capacity and the adsorption rate constant by using the Thomas model, which is one of the most general and widely used models for column performance evaluation [39]. The Thomas model is expressed as follows:

$$\frac{c_t}{c_0} = \frac{1}{1 + \exp\left(\frac{k_{Th}q_0x}{v} - k_{Th}c_0t\right)} \qquad (6)$$

where k_{Th} is the Thomas rate constant (mL/min·mg); q_0 is the equilibrium Cs uptake per gram of the adsorbent (mg/g); x is the amount of adsorbent in the column (g); c_0 is the influent Cs concentration (mg/L); and v is the flow rate (mL/min).

3. Results and discussion

3.1. Adsorbent characterization

3.1.1. SEM–EDS analysis

The morphological changes of GAC after the surface modification

Table 1
Composition of water samples used in the experiments.

	Soft water (µeq/l)	Hard water (µeq/l)	Real stream water (µeq/l)
Mg^{2+}	120	815	787
Ca^{2+}	530	2450	1498
Na^+	250	665	1274
K^+	25	105	160
Cl^-	280	685	1292
NO_3^-	30	100	247
SO_4^{2-}	230	1210	874
$H_2PO_4^-$	–	30	–
HCO_3^-	385	2010	1300

and the PB immobilization steps were monitored via SEM observation. Fig. 2 compares the morphology of the GAC-Ox, GAC-COP, and GAC-COP-PB samples. The pristine GAC-Ox showed a generally smooth surface with many tiny pores and debris. In the GAC-COP case, another material was newly formed on the GAC surface; its higher-magnification image revealed a chain structure typical of polymers, with spherical particles intertwined like a net. These results are consistent with the GAC-COP structure reported in previous studies, indicating the successful COP growth on the GAC surface [33]. The changes in textural and chemical properties during COP growth on the AC surface were reported in our previous studies [31,33]. The GAC-COP-PB composite exhibited a similar chain structure, but the surface brightness significantly increased due to PB's metallicity; furthermore, we observed a cubic form of PB attached to the round polymer structure. The cubic morphology of PB was observed in the porous COP network.

The corresponding EDS results are summarized in Table 2. The GAC-Ox contained 89.6% carbon, which is the typical composition of GAC, and some oxygen was also detected due to the presence of the –OH groups. After the COP grafting, the carbon amount was significantly reduced and the nitrogen signal appeared; this confirms that the GAC was successfully grafted since N is a constituent element of the COP used. Moreover, the increased oxygen content resulted from the acid treatment during COP grafting. Both GAC-COP-PB and GAC-PB exhibited the presence of iron due to the molecular structure of PB. However, the iron content was 1.8 times higher in GAC-COP-PB than in GAC-PB, demonstrating that the COP grafting promoted the PB immobilization. The PB immobilization was enhanced due to the coordination bonding between the electron-rich amine groups and ferric ions. A similar promotion effect of COP on iron adsorption was mentioned in our previous study on the immobilization of nanoscale zero-valent iron on GAC-COP [33]. We expected the PB to be located in the COP network, as confirmed in our previous study by using SEM-EDS mapping to investigate the location of Fe in the composite [28]. Based on the chemical formula of PB, the PB content in GAC-COP-PB was nearly 13.1% of the total weight.

3.1.2. FTIR analysis

The FTIR spectra are shown in Fig. 3. The GAC-Ox exhibited peaks at 1320–1000 and 3550–3200 cm^{-1} corresponding to the oxygen-containing functional groups (C–O, and O–H, respectively). This was ascribed to GAC oxidation because pristine GAC generally shows almost no FTIR peaks [30]. After the COP grafting, a new peak appeared at 1625 cm^{-1} and attributed to the N–H bending in the amine groups of the COP structure [40]. The FTIR pattern was similar to those previously reported COP-grafted powdered activated carbon [31], further confirming the successful COP grafting on the GAC surface. Both the GAC-PB and GAC-COP-BP samples exhibited also a new peak at 2080 cm^{-1}, attributed to C≡N, indicating the successful immobilization of PB [41].

3.2. Effects of COP grafting on the stable PB immobilization

The effects of COP grafting on the PB immobilization and subsequent cesium adsorption were evaluated via an adsorption test (Fig. 4). The pristine GAC exhibited a limited ^{133}Cs removal efficiency, similarly to the GAC-COP; this indicates that the COP grafting did not significantly enhance the cesium adsorption capacity. In comparison, the GAC-PB showed an improved adsorption efficiency, probably due to the contribution of the immobilized PB. The highest efficiency was achieved by the GAC-COP-PB, confirming the effectiveness of the COP grafting in stabilizing the PB immobilization; the efficiency was approximately three times more than that of the GAC-PB. This indicates that the cesium adsorption ability of GAC-COP-PB was due to PB and not to the supporting material or surface modification.

The stability of the PB immobilization was evaluated based on the PB detachment (Fig. 3(b)). The GAC-PB and GAC-COP-PB were mixed with deionized water for 24 h at 200 rpm, and the amount of PB eluted after
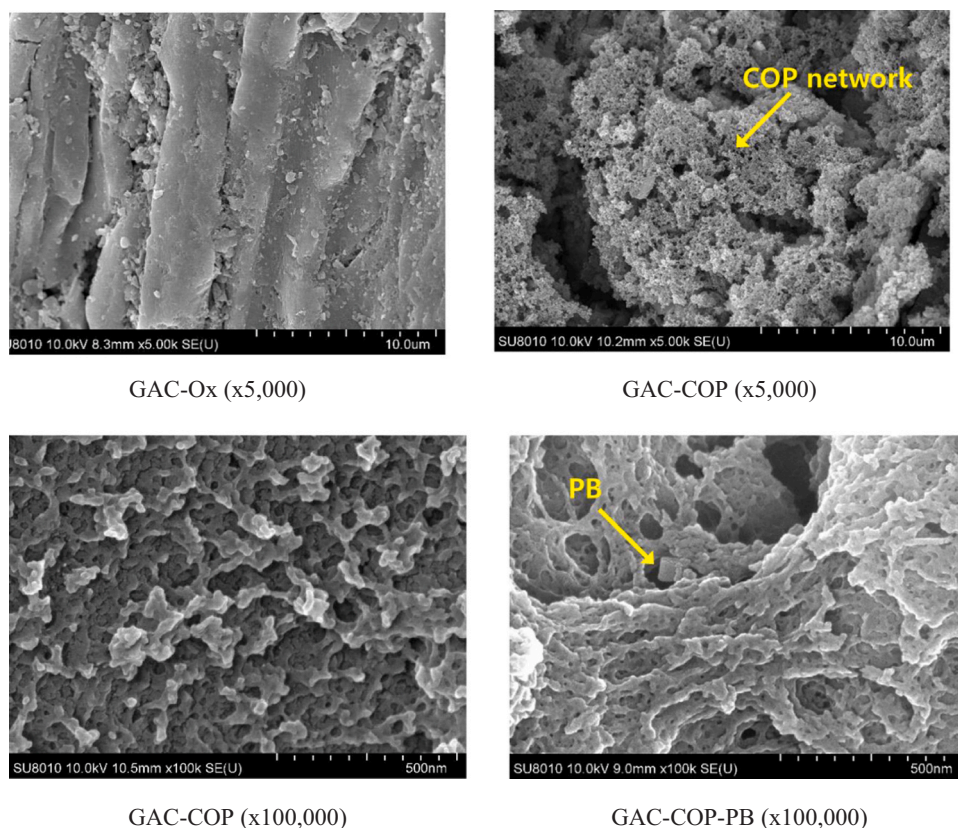
GAC-Ox (x5,000)

GAC-COP (x5,000)

GAC-COP (x100,000)

GAC-COP-PB (x100,000)

Fig. 2. Scanning electron micrographs of granular activated carbon (GAC), covalent organic polymer-grafted GAC (GAC-COP), and Prussian blue-immobilized GAC-COP (GAC-COP-PB).

Table 2
Elemental composition obtained by means of SEM-EDS analysis.

Adsorbent	Element (Weight%)			
	C	N	O	Fe
GAC-Ox (n = 1)	89.60	–	10.40	–
GAC-COP (n = 4)	58.37 ± 6.56	12.46 ± 1.04	17.15 ± 3.85	–
GAC-PB (n = 3)	70.88 ± 6.13	–	19.69 ± 3.23	3.26 ± 0.38
GAC-COP-PB (n = 2)	54.32 ± 3.94	18.31 ± 1.33	16.53 ± 1.20	5.98 ± 0.43

stirring was measured via spectroscopic analysis. The PB desorption increased along with the concentration of adsorbent added. The degree of PB desorption was 2–2.5 times higher for GAC-PB than for GAC-COP-PB. Considering that the GAC-COP-PB contained approximately 1.9

times more PB than the GAC-PB, this result indicates that the COP grafting successfully minimized the PB desorption, stabilizing the PB immobilization; therefore, we expected a higher cesium adsorption efficiency as well. The amount of PB detached during the 24-h test was calculated to be less than 0.01% of the immobilized PB.

3.3. Adsorption kinetics

The equilibrium time between the adsorbents and the cesium solution was determined by performing a kinetic adsorption test. Fig. 5 shows a plot of the observed adsorption capacity as a function of time; the experimental data were fitted using Eqs. (2) and (3). The corresponding kinetic parameters are summarized in Table 3.

The amount of cesium adsorbed increased rapidly during the first 3 h; after 24 h, it almost stabilized, and at this time, the adsorption capacities computed using the pseudo-second-order kinetics of GAC-COP-
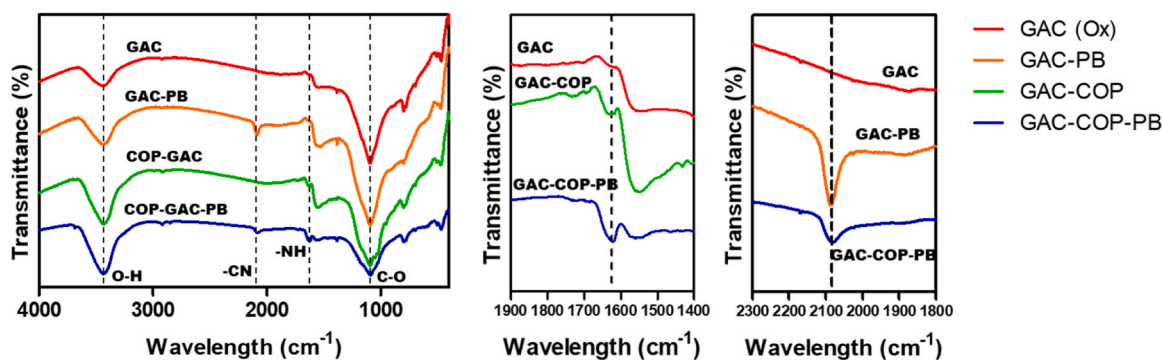

Fig. 3. Fourier-transform infrared spectra of oxidized granular activated carbon (GAC-Ox), Prussian blue-immobilized GAC (GAC-PB), covalent organic polymer-grafted GAC (GAC-COP), and Prussian blue-immobilized GAC-COP (GAC-COP-PB).
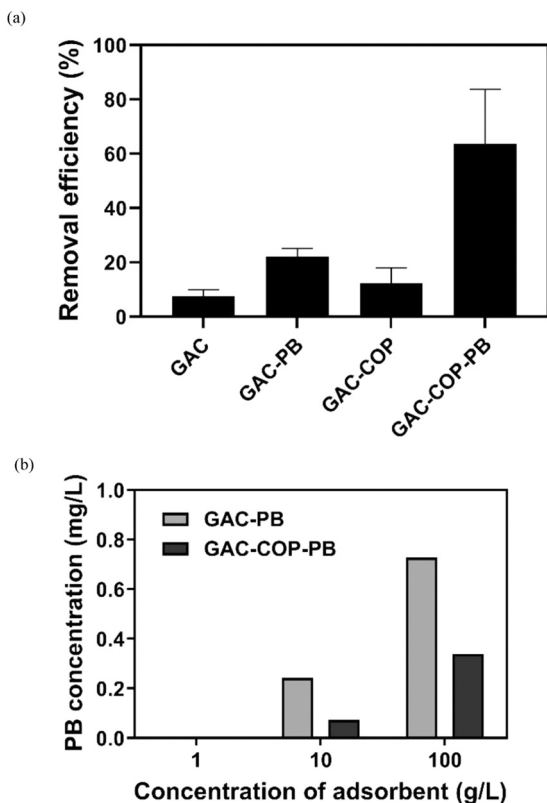
(a)

(b)

Fig. 4. (a) ^{133}Cs removal efficiency of and (b) amount of Prussian blue (PB) detached from granular activated carbon (GAC), Prussian blue-immobilized GAC (GAC-PB), covalent organic polymer-grafted GAC (GAC-COP), and Prussian blue-immobilized GAC-COP (GAC-COP-PB).
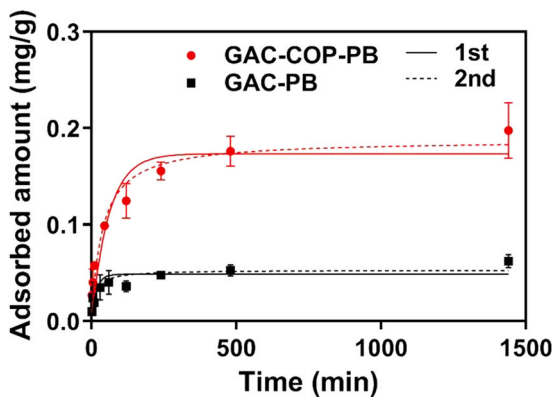

Fig. 5. Pseudo-first-order (solid line) and pseudo-second-order (dashed line) fittings of the amounts of cesium adsorbed on the Prussian-blue-immobilized granular activated carbon (GAC-PB) and Prussian-blue-immobilized covalent organic polymer-grafted GAC (GAC-COP-PB).

Table 3
Kinetic model parameters of cesium adsorption by Prussian-blue-immobilized granular activated carbon (GAC-PB) and Prussian-blue-immobilized covalent organic polymer-grafted GAC (GAC-COP-PB).

	Material	q_e (mg/g)	k_1 or k_2	R^2
Pseudo-first-order	GAC-COP-PB	0.1735	0.0167	0.8396
	GAC-PB	0.0486	0.0585	0.5655
Pseudo-second-order	GAC-COP-PB	0.1877	0.1415	0.9062
	GAC-PB	0.0528	1.444	0.6639

PB and GAC-PB were 0.1877 and 0.0528 mg/g, respectively. These results imply that the adsorption capacity of GAC-COP-PB was 3.6 times higher than that of GAC-PB. The q_e values calculated using the pseudo-first-order kinetic exhibited a similar tendency.

The kinetic constants of the unmodified GAC-PB were relatively higher, suggesting that the pores were blocked to some extent by the COP grafting. The lower kinetic constants of the GAC-COP-PB affected the initial adsorption phase. Because the adsorption equilibrium was reached after 3–8 h of adsorption time, we used an adsorption time of 24 h in the following equilibrium experiments.

3.4. Adsorption isotherms

The cesium adsorption capacities of GAC-PB and GAC-COP-PB were compared via adsorption isotherm experiments; the experimental data were fitted with Langmuir and Freundlich equations (Fig. 6 and Table 4).

Generally, the GAC-COP-PB exhibited much higher cesium adsorption capacity than the GAC-PB. The Langmuir q_m values of GAC-PB and GAC-COP-PB, 0.3455 mg/g and 1.091 mg/g, indicates that the overall adsorption capacity was increased around 3.2 times through the surface functionalization with COP, which stabilized the PB immobilization, increasing the PB content in the adsorbent and, finally, improving its adsorption capacity. The q_m value normalized against the PB content determined by means of EDS analysis was calculated to be 8.33 mg/g PB. The PB entrapped in the alginate beads exhibited a similar adsorption capacity of 3.33–43.5 mg/g in the concentration range of 45–100 mg/L [26,42]. Furthermore, the dimensionless constant, that is, the separation factor (R_L), was calculated using Eq. (7) [37]:

$$R_L = \frac{1}{1 + K_L c_0} \tag{7}$$

where C_0 is the highest initial concentration of the adsorbate (mg/L),
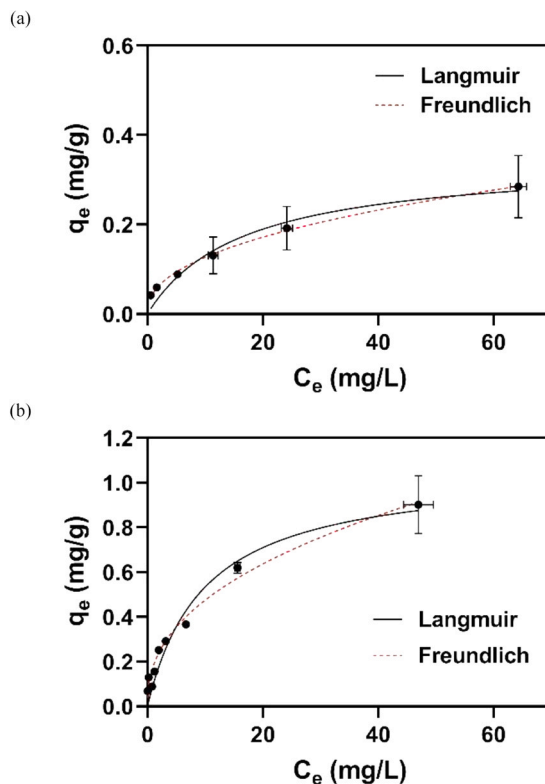
(a)

(b)

Fig. 6. ^{133}Cs adsorption isotherm with (a) Prussian-blue-immobilized granular activated carbon (GAC-PB) and (b) Prussian-blue-immobilized covalent organic polymer-grafted GAC (GAC-COP-PB).

Table 4

Adsorption isotherm model parameters of Prussian-blue-immobilized granular activated carbon (GAC-PB) and Prussian-blue-immobilized covalent organic polymer-grafted GAC (GAC-COP-PB).

| Adsorbent	Langmuir isotherm			Freundlich isotherm		
	q_m (mg/g)	K_L (L/mg)	R^2	K_F	n	R^2
GAC-COP-PB	1.091	0.0910	0.9324	0.1949	2.507	0.9737
GAC- PB	0.3455	0.0608	0.8573	0.0465	2.295	0.9013

and K_L is the Langmuir constant (L/mg). The value of R_L indicates the shape of the isotherm as being unfavorable ($R_L > 1$), linear ($R_L = 1$), favorable ($0 < R_L < 1$), or irreversible ($R_L = 0$). The R_L values in the present investigation were 0.767 and 0.687 for GAC-PB and GAC-COP-PB, respectively, indicating that the adsorption of cesium on the prepared adsorbents was favorable.

The Freundlich isotherm, an empirical equation used to describe heterogeneous systems, was applied to interpret the adsorption data (Eq. 5). The magnitude of the exponent, $1/n$, indicates the favorability of adsorption. The values of n in the present investigation were 2.295 and 2.507 for GAC-PB and GAC-COP-PB, respectively, indicating a favorable adsorption condition ($n > 1$) [37].

Cesium adsorption on PB is driven by both physisorption and chemisorption. Ishizaki et al. attributed the PB exclusive ability to adsorb hydrated cesium ions into its regular lattice spaces surrounded by cyanide-bridged metals [22]. In Prussian blue ($Fe_4[Fe(CN)_6]_3 \cdot xH_2O$), many defect sites (vacant spaces) of $[Fe(CN)_6]^{4-}$ are filled with coordination and crystallization water molecules because the number of the latter ones is high. A similar approach and explanation are available in literature [13,24].

3.5. Effect of pH

The pH role in metal adsorption is greatly important since it influences both the binding sites and the metal speciation. We investigated this study aspect for GAC-COP-BP by varying the initial pH. Fig. 7 illustrates the pH values before and after 24 h of adsorption time, as along with the corresponding amounts of adsorbed ^{133}Cs. The final pH was lower than the initial one in all the cases, and its decrease became more significant when increasing the initial pH. This pH reduction could be explained by the following reaction [22].

$$Fe^{III} - OH_2 + Cs^+A^- \rightarrow \{Fe^{III} - OH\}^- Cs^+ + H^+A^- \qquad (8)$$
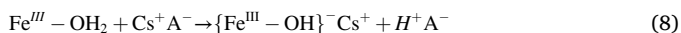
The initial and final pH values were closely related to the cesium adsorption capacity; higher adsorption capacities were obtained in weak alkaline conditions. When the pH increased from 6 to 8, the adsorption efficiency increased by about 19%, reaching its maximum. Since Cs^+ is the predominant species in the entire pH range [43], the pH effect cannot be explained by its speciation of Cs^+ at different pH values.
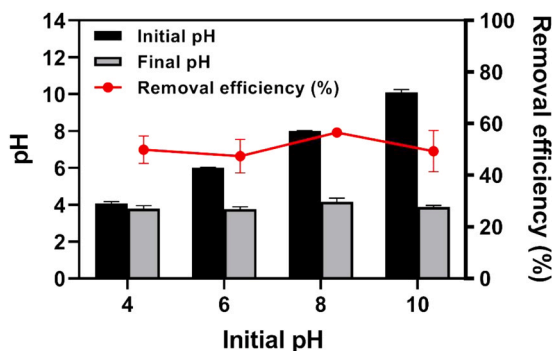
Therefore, the lower performance observed under acidic conditions resulted from the competition between H^+ and Cs^+, as reported in previous works [44,45]. pH strongly influences ion-exchange processes, especially those involving monovalent cations, because of the competition for ion exchange with protons. At low pH values, the ion exchange sites are mainly protonated and, thus, less available for the cations [13]. At very high pH values, the hydroxide ions dissolve the Fe–(CN)–Fe bond of the PB, disrupting its lattice structure and, hence, reducing its adsorption efficiency [46].

3.6. Effect of water matrix

We investigated the water matrix effect to evaluate the practical applicability of GAC-COP-PB for environmental media containing interfering substances. Fig. 8 shows the measured cesium removal efficiency and pH variation The ^{133}Cs removal efficiencies of the deionized, soft, hard, and real stream water samples were approximately 47%, 57%, 68%, and 75%, respectively; interestingly, the adsorption efficiency increased in the presence of competing cations.

The Cs adsorption by PB is governed by three mechanisms: ion exchange between Cs^+ and K^+, Cs^+ percolation through the PB surface vacancies, and proton exchange with Cs^+. The excellent selectivity that we observed for Cs is mainly due to the complete dehydration of the alkali cations during the ion exchange. Besides, the difference between the energy of the hydrated states of K^+ (-351.8 kJ/mol) and Cs^+ (-306.4 kJ/mol) is the main driving force for the ion exchange (Cs^+ adsorption) [24]. Our experimental results are consistent with previous reports in terms of selectivity [47].

The GAC-COP-PB exhibited the best ^{133}Cs removal performance in the real stream water sample. Moreover, its absorption efficiency was higher in hard water than in soft water. These results should be discussed considering the pH variation during the adsorption. As described above, the pH was decreased by the H^+ released via ion exchange, preventing further cesium adsorption. The HCO_3^- content in the real stream and hard water samples was high compared to those in deionized and soft water ones. Thus, the pH change was minimized for the real stream water and hard water samples, as shown in Fig. 8. All these results demonstrate the high selectivity of GAC-COP-PB toward cesium and, thus, its applicability for treating real water streams.

3.7. Continuous column experiment

We evaluated the feasibility of GAC-COP-PB for water treatment by conducting a continuous column test. Moreover, we used a column filled with GAC-PB as the control. The flow rate was adjusted from 0.2 mL/min to 2.0 mL/min, and the experimental results are shown and summarized in Fig. 9 and Table 5, respectively. The experimental results were fitted using the Thomas equation as well.
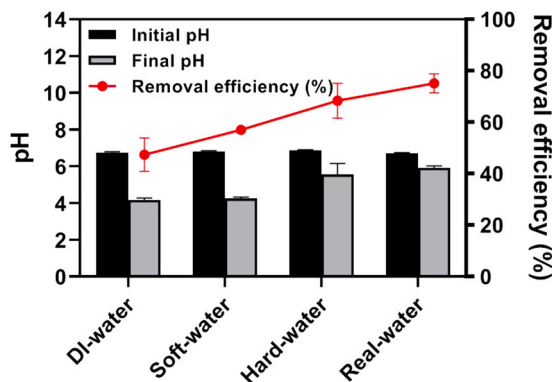

Fig. 7. Effect of initial pH on cesium adsorption efficiency of Prussian blue-immobilized covalent organic polymer-grafted GAC (GAC-COP-PB).

Fig. 8. Effect of water matrix on the cesium adsorption efficiency of Prussian blue-immobilized covalent organic polymer-grafted GAC (GAC-COP-PB).

At the high flow rate of 2.0 mL/min, column breakthrough occurs almost instantly after the column experiment. In the GAC-PB case, the cesium concentration in the first sample extracted after 10 min was 4.9 μg/L, which corresponded to a removal efficiency of 97.6%. However, the removal efficiency decreased to 30% within 1 h and further decreased to 10% within a day. The GAC-COP-PB yielded superior results owing to its higher PB loading. The removal efficiency in the first sample was 99.0%, which decreased to 67% within 1 h, and remained at 32% after 36 h. The Thomas equation was not appropriate for interpreting the results obtained in this high-flow-rate case ($R^2 < 0.7$); therefore, we calculated the amount of cesium removed by using the area above the curve. The overall amounts of cesium removed by the GAC-PB and the GAC-COP-PB over 24 h were 132 and 267 μg, respectively, which corresponded to 23.0% and 46.3% of the ^{133}Cs added to the column (0.002 L/min × 200 μg/L × 1440 min = 576 μg). The amounts of cesium removed per unit adsorbent mass were calculated as 0.044 mg/g and 0.089 mg/g for GAC-PB and GAC-COP-PB, respectively. The removal efficiency of GAC-COP-PB was approximately twice that of GAC-PB, which is similar to the difference in their PB loadings.

At the low flow rate of 0.2 mL/min, the Thomas equation successfully interpreted the overall column operation results. The column could be operated for a considerably longer time compared to that in the high-flow-rate condition, and the performance of the GAC-COP-PB was superior to that of the GAC-PB. The q_0 values obtained using the Thomas equation were 0.095 mg/g and 0.179 mg/g for the GAC-PB and the GAC-COP-PB, respectively. These results clearly indicated the effect of flow rate on column operation. When the column was operated at a low flow rate, the contact time between the adsorbate and the adsorbent was longer; therefore, higher removal efficiencies were achieved. Under our experimental conditions, the contact time was 2.5 min under the high-flow-rate condition (2.0 mL/min) and 25 min under the low-flow-rate condition (0.2 mL/min), which are considerably shorter than the adsorption equilibrium times achieved in the kinetic test (1–6 h). Similar results related to the effect of the flow rate on the adsorbent column have been reported by other researchers, and it has generally been explained on the basis of mass transfer fundamentals [39,48]. These results confirmed the potential of GAC-COP-PB for removing radioactive cesium from contaminated streams by optimizing the contact time and column loading.

4. Conclusion

We prepared a filling material for separation columns based on PB as the active cesium adsorbent. The commercially available GAC was selected as the supporting material to reduce the fabrication costs and its surface was grafted with a COP to improve the PB immobilization via both physical entrapment and chemical interactions between amine groups and ferric ions. The beneficial effect of COP grafting was demonstrated through PB detachment, FTIR, and SEM–EDS analyses. Compared to pristine GAC, the prepared GAC-COP immobilized approximately 1.9 times more PB and exhibited a higher cesium adsorption efficiency. Then, the adsorption isotherm test results fitted using the Langmuir model revealed a maximum ^{133}Cs adsorption capacity of 1.091 mg/g for GAC-COP-PB, which was 3.2 times higher than that of GAC-PB; the q_m value normalized by the PB loading was 8.33 mg/g PB. The adsorption behavior depended on the initial pH and buffering. The best performance was obtained in an alkaline pH range, while the water matrix did not hinder the adsorption capacity. Finally, we conducted a continuous adsorption experiment with different flow rates, and the removal performance of the GAC-COP-PB was approximately twice as good as that of the GAC-PB. The GAC-COP-PB column was successfully operated for 255 h with a cumulative removal efficiency of 76.5% under the flow rate of 0.2 mL/min. The optimization of column operation, as well as verification with ^{137}Cs, will further demonstrate the potential of the proposed material for use as a column filler toward the remediation of radioactive cesium.
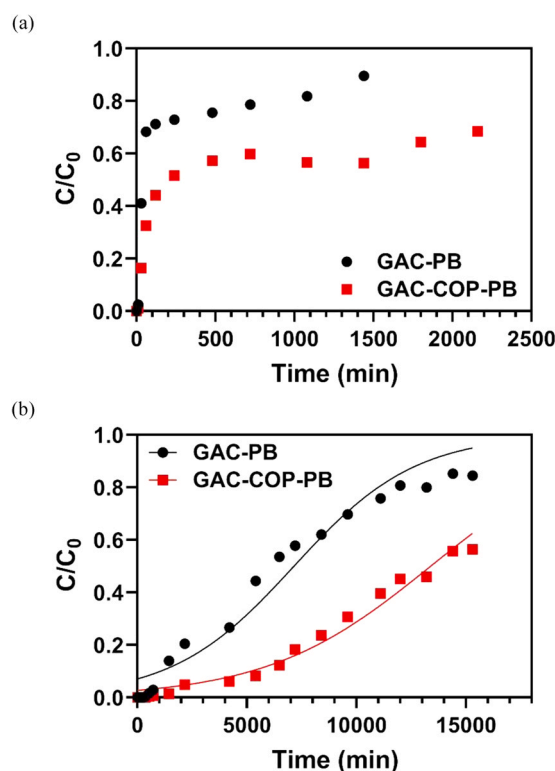

Fig. 9. ^{133}Cs concentration profile in the effluent during the column experiment with different flow rates. (a) 2.0 mL/min and (b) 0.2 mL/min.

Table 5
Model parameters obtained by performing nonlinear regression analysis using the Thomas model for cesium adsorption onto Prussian-blue-immobilized granular activated carbon (GAC-PB) and Prussian-blue-immobilized covalent organic polymer-grafted GAC (GAC-COP-PB).

Flow rate (mL/min)	GAC-PB			GAC-COP-PB		
	q_0 (mg/g)	k_{Th} (mL/min·mg)	R^2	q_0 (mg/g)	k_{Th} (mL/min·mg)	R^2
0.2	0.0954	1.804	0.9571	0.1786	1.339	0.9764
2	0.0061	261.4	0.6595	0.1285	5.021	0.5431

CRediT authorship contribution statement

Younggyo Seo: Investigation, Writing - original draft. **Yuhoon Hwang**: Conceptualization, Writing - review & editing.

Declaration of Competing Interest

The authors declare that they have no known competing financial interests or personal relationships that could have appeared to influence the work reported in this paper.

References

[1] M.S. Dresselhaus, I.L. Thomas, Alternative energy technologies, Nature 414 (2001) 332–337.

[2] C.W. Forsberg, Sustainability by combining nuclear, fossil, and renewable energy sources, Prog. Nucl. Energy 51 (2009) 192–200.

[3] International Energy Agency, World Energy Statistics 2018, 2018.

[4] H. Tsuji, T. Yasutaka, Y. Kawabe, T. Onishi, T. Komai, Distribution of dissolved and particulate radiocesium concentrations along rivers and the relations between radiocesium concentration and deposition after the nuclear power plant accident in Fukushima, Water Res. 60 (2014) 15–27.

[5] M. Ebihara, N. Yoshida, Y. Takahashi, Preface: migration of radionuclides from the Fukushima Daiichi Nuclear Power Plant accident, Geochem. J. 46 (2012) 267–270.

[6] M.A. Olatunji, M.U. Khandaker, Mahmud, H. N. M. E, Y.M. Amin, Influence of adsorption parameters on cesium uptake from aqueous solutions- a brief review, RSC Adv. 5 (2015) 71658–71683.

[7] A. El-Kamash, Evaluation of zeolite A for the sorptive removal of Cs+ and Sr2+ ions from aqueous solutions using batch and fixed bed column operations, J. Hazard. Mater. 151 (2008) 432–445.

[8] F. Jia, J. Wang, Separation of cesium ions from aqueous solution by vacuum membrane distillation process, Prog. Nucl. Energy 98 (2017) 293–300.

[9] A.G. Chmielewski, M. Harasimowicz, B. Tyminski, G. Zakrzewska-Trznadel, Concentration of low- and medium-level radioactive wastes with three-stage reverse osmosis pilot plant, Sep. Sci. Technol. 36 (2001) 1117–1127.

[10] A. Nilchi, R. Saberi, M. Moradi, H. Azizpour, R. Zarghami, Adsorption of cesium on copper hexacyanoferrate–PAN composite ion exchanger from aqueous solution, Chem. Eng. J. 172 (2011) 572–580.

[11] S. Ding, Y. Yang, C. Li, H. Huang, L. Hou, The effects of organic fouling on the removal of radionuclides by reverse osmosis membranes, Water Res. 95 (2016) 174–184.

[12] V. Tricoli, Proton and methanol transport in poly(perfluorosulfonate) membranes containing Cs + and H+ cations, J. Electrochem. Soc. 145 (2019) 3798–3801.

[13] A.K. Vipin, B. Hu, B. Fugetsu, Prussian blue caged in alginate/calcium beads as adsorbents for removal of cesium ions from contaminated water, J. Hazard. Mater. 258–259 (2013) 93–101.

[14] G. Chen, Y. Chang, X. Liu, T. Kawamoto, H. Tanaka, A. Kitajima, D. Parajuli, M. Takasaki, K. Yoshino, M. Chen, Y. Lo, Z. Lei, D. Lee, Prussian blue (PB) granules for cesium (Cs) removal from drinking water, Sep. Purif. Technol. 143 (2015) 146–151.

[15] D. Ding, Z. Zhang, R. Chen, T. Cai, Selective removal of cesium by ammonium molybdophosphate – polyacrylonitrile bead and membrane, J. Hazard. Mater. 324 (2017) 753–761.

[16] K. Lee, K. Kim, M. Park, J. Kim, M. Oh, E. Lee, D. Chung, J. Moon, Novel application of nanozeolite for radioactive cesium removal from high-salt wastewater, Water Res. 95 (2016) 134–141.

[17] A.A. Kadam, J. Jang, D.S. Lee, Facile synthesis of pectin-stabilized magnetic graphene oxide Prussian blue nanocomposites for selective cesium removal from aqueous solution, Bioresour. Technol. 216 (2016) 391–398.

[18] C. Delchet, A. Tokarev, X. Dumail, G. Toquer, Y. Barré, Y. Guari, C. Guerin, J. Larionova, A. Grandjean, Extraction of radioactive cesium using innovative functionalized porous materials, RSC Adv. 2 (2012) 5707–5716.

[19] P.A. Haas, A review of information on ferrocyanide solids for removal of cesium from solutions, Sep. Sci. Technol. 28 (1993) 2479–2506.

[20] B. Kong, J. Tang, Z. Wu, J. Wei, H. Wu, Y. Wang, G. Zheng, D. Zhao, Ultralight mesoporous magnetic frameworks by interfacial assembly of Prussian blue nanocubes, in: Angew. Chem. Int. Ed, 53, 2014, pp. 2888–2892.

[21] H.J. Buser, D. Schwarzenbach, W. Petter, A. Ludi, The crystal structure of Prussian blue: Fe4[Fe(CN)6]3.xH2O, Inorg. Chem. 16 (1977) 2704–2710.

[22] M. Ishizaki, S. Akiba, A. Ohtani, Y. Hoshi, K. Ono, M. Matsuba, T. Togashi, K. Kananizuka, M. Sakamoto, A. Takahashi, T. Kawamoto, H. Tanaka, M. Watanabe, M. Arisaka, T. Nankawa, M. Kurihara, Proton-exchange mechanism of specific Cs+ adsorption via lattice defect sites of Prussian blue filled with coordination and crystallization water molecules, Dalton Trans. 42 (2013) 16049–16055.

[23] H.A. Alamudy, K. Cho, Selective adsorption of cesium from an aqueous solution by a montmorillonite-Prussian blue hybrid, Chem. Eng. J. 349 (2018) 595–602.

[24] A. Takahashi, H. Tanaka, K. Minami, K. Noda, M. Ishizaki, M. Kurihara, H. Ogawa, T. Kawamoto, Unveiling Cs-adsorption mechanism of Prussian blue analogs: Cs+-percolation via vacancies to complete dehydrated state, RSC Adv. 8 (2018) 34808–34816.

[25] H. Kim, M. Kim, W. Lee, S. Kim, Rapid removal of radioactive cesium by polyacrylonitrile nanofibers containing Prussian blue, J. Hazard. Mater. 347 (2018) 106–113.

[26] H. Yang, H. Li, J. Zhai, L. Sun, Y. Zhao, H. Yu, Magnetic Prussian blue/graphene oxide nanocomposites caged in calcium alginate microbeads for elimination of cesium ions from water and soil, Chem. Eng. J. 246 (2014) 10–19.

[27] J. Kiener, L. Limousy, M. Jeguirim, J. Le Meins, S. Hajjar-Garreau, G. Bigoin, C. M. Ghimbeu, Activated carbon/transition metal (Ni, In, Cu) hexacyanoferrate nanocomposites for cesium adsorption, in: Materials (Basel, Switzerland), 12, 2019, p. 1253.

[28] Younggyo Seo, Daemin Oh, Yuhoon Hwang, Covalent organic polymer grafted on granular activated carbon surface to immobilize Prussian blue for Cs+ removal, J. Korean Soc. Water Wastewater 32 (2018) 399–409 (Korean Society Of Water And Wastewater).

[29] H. Kim, H. Wi, S. Kang, S. Yoon, S. Bae, Y. Hwang, Prussian blue immobilized cellulosic filter for the removal of aqueous cesium, Sci. Total Environ. 670 (2019) 779–788.

[30] H. Wi, H. Kim, D. Oh, S. Bae, Y. Hwang, Surface modification of poly(vinyl alcohol) sponge by acrylic acid to immobilize Prussian blue for selective adsorption of aqueous cesium, Chemosphere 226 (2019) 173–182.

[31] P.D. Mines, D. Thirion, B. Uthuppu, Y. Hwang, M.H. Jakobsen, H.R. Andersen, C. T. Yavuz, Covalent organic polymer functionalization of activated carbon surfaces through acyl chloride for environmental clean-up, Chem. Eng. J. 309 (2017) 766–771.

[32] B. Kim, D. Oh, S. Kang, Y. Kim, S. Kim, Y. Chung, Y. Seo, Y. Hwang, Reformation of the surface of powdered activated carbon (PAC) using covalent organic polymers (COPs) and synthesis of a Prussian blue impregnated adsorbent for the decontamination of radioactive cesium, J. Alloy. Compd. 785 (2019) 46–52.

[33] P.D. Mines, B. Uthuppu, D. Thirion, M.H. Jakobsen, C.T. Yavuz, H.R. Andersen, Y. Hwang, Granular activated carbon with grafted nanoporous polymer enhances nanoscale zero-valent iron impregnation and water contaminant removal, Chem. Eng. J. 339 (2018) 22–31.

[34] S. Khandaker, Y. Toyohara, S. Kamida, T. Kuba, Adsorptive removal of cesium from aqueous solution using oxidized bamboo charcoal, Water Resour. Ind. 19 (2018) 35–46.

[35] D. Ko, J.S. Lee, H.A. Patel, M.H. Jakobsen, Y. Hwang, C.T. Yavuz, H.C.B. Hansen, H.R. Andersen, Selective removal of heavy metal ions by disulfide linked polymer networks, J. Hazard. Mater. 332 (2017) 140–148.

[36] K.Y. Foo, B.H. Hameed, Insights into the modeling of adsorption isotherm systems, Chem. Eng. J. 156 (2010) 2–10.

[37] B.H. Hameed, J.M. Salman, A.L. Ahmad, Adsorption isotherm and kinetic modeling of 2,4-D pesticide on activated carbon derived from date stones, J. Hazard. Mater. 163 (2009) 121–126.

[38] E.J. Smith, W. Davison, J. Hamilton-Taylor, Methods for preparing synthetic freshwaters, Water Res. 36 (2002) 1286–1296.

[39] R. Han, Y. Wang, W. Zou, Y. Wang, J. Shi, Comparison of linear and nonlinear analysis in estimating the Thomas model parameters for methylene blue adsorption onto natural zeolite in fixed-bed column, J. Hazard. Mater. 145 (2007) 331–335.

[40] H.A. Patel, C.T. Yavuz, Highly optimized CO2 capture by inexpensive nanoporous covalent organic polymers and their amine composites, Faraday Discuss. 183 (2015) 401–412.

[41] P.J. Kulesza, M.A. Malik, A. Denca, J. Strojek, In Situ FT-IR/ATR Spectroelectrochemistry of Prussian Blue in the Solid State, Anal. Chem. 68 (1996) 2442–2446.

[42] Y. Lai, Y. Chang, M. Chen, Y. Lo, J. Lai, D. Lee, Poly(vinyl alcohol) and alginate cross-linked matrix with immobilized Prussian blue and ion exchange resin for cesium removal from waters, Bioresour. Technol. 214 (2016) 192–198.

[43] M.M. Hamed, M. Holiel, I.M. Ahmed, Sorption behavior of cesium, cobalt and europium radionuclides onto hydroxyl magnesium silicate, Radiochim. Acta 104 (2016) 873–890.

[44] S. Feng, X. Li, F. Ma, R. Liu, G. Fu, S. Xing, X. Yue, Prussian blue functionalized microcapsules for effective removal of cesium in a water environment, RSC Adv. 6 (2016) 34399–34410.

[45] H. Yang, J.R. Hwang, D.Y. Lee, K.B. Kim, C.W. Park, H.R. Kim, K. Lee, Eco-friendly one-pot synthesis of Prussian blue-embedded magnetic hydrogel beads for the removal of cesium from water, Sci. Rep. 8 (2018) 11476.

[46] A.A. Karyakin, E.E. Karyakina, L. Gorton, On the mechanism of H2O2 reduction at Prussian Blue modified electrodes, Electrochem. Commun. 1 (1999) 78–82.

[47] S. Jang, S. Kang, Y. Haldorai, K. Giribabu, G. Lee, Y. Lee, M.S. Hyun, Y. Han, C. Roh, Y.S. Huh, Synergistically strengthened 3D micro-scavenger cage adsorbent for selective removal of radioactive cesium, Sci. Rep. 6 (2016) 38384.

[48] D.C.K. Ko, J.F. Porter, G. McKay, Optimised correlations for the fixed-bed adsorption of metal ions on bone char, Chem. Eng. Sci. 55 (2000) 5819–5829.